ISSN 0026-8933, Molecular Biology, 2024, Vol. 58, No. 6, pp. 1280–1292. © Pleiades Publishing, Ltd., 2024.

STRUCTURAL-FUNCTIONAL ANALYSIS OF BIOPOLYMERS AND THEIR COMPLEXES

UDC 616-006

N-Acetylgalactosamine-Conjugated Antisense Oligonucleotides Designed as Inhibitors of ABCB1: Coping with Multidrug Resistance in Hepatocellular Carcinoma

B. Hasturk[a] (ORCID: 0000-0001-8790-144X), T. Avsar[b, c] (ORCID: 0000-0001-8841-4811), S. Ozbas[d] (ORCID: 0000-0002-1721-7543), B. Karademir Yilmaz[e, f] (ORCID: 0000-0003-1762-0284), and F. Eren[g, h, *] (ORCID: 0000-0001-8126-2413)

[a] *Marmara University, Institute of Health Sciences, Department of Medical Biology and Genetics, Istanbul, 34854 Turkey*
[b] *Bahçeşehir University; School of Medicine, Department of Medical Biology, Istanbul, 34734 Turkey*
[c] *Bahçeşehir University, Health Sciences Institute, Neuroscience Laboratory, Istanbul, 34734 Turkey*
[d] *Marmara University, Faculty of Pharmacy, Department of Pharmaceutical Biotechnology, Istanbul, 34854 Turkey*
[e] *Marmara University, Faculty of Medicine, Department of Medical Biochemistry, Istanbul, 34854 Turkey*
[f] *Marmara University, Genetic and Metabolic Diseases Research and Investigation Center (GEMHAM), Istanbul, 34854 Turkey*
[g] *Marmara University, Faculty of Medicine, Department of Medical Biology, Istanbul, 34854 Turkey*
[h] *Marmara University, Institute of Gastroenterology, Liver Research Unit, Istanbul, 34854 Turkey*
**e-mail: erenfatih78@yahoo.com*

Received March 28, 2024; revised July 17, 2024; accepted July 26, 2024

Abstract—Cancer-multidrug resistance (MDR) is recognized as one of the barriers to the treatment of advanced hepatocellular carcinoma (HCC). We aim to inhibit ABCB1 overexpression observed in HCC-MDR phenotypes with *N*-acetylgalactosamine (GalNAc)-conjugated antisense oligonucleotides (ASOs). In this study, three ASOs (GalNAc-ASO1, GalNAc-ASO2, and GalNAc-ASO3) targeting ABCB1 mRNA and a scrambled-negative control (GalNAc-ASO4) were designed. Simulations of molecular docking were performed to determine the inhibitory efficacy of ASOs. GalNAc C3 phosphoramide ligand was added to the 5'-end of the ASO sequences, and phosphorothioate modifications were added to the DNA backbone. HepG2 cells were directly treated with different doses of GalNAc-ASOs conjugates. To evaluate the inhibitory effect of GalNAc-ASOs conjugates, the protein level of ABCB1 was measured by western blotting. The cell viability assays of GalNAc-ASO4 conjugates on HepG2 were evaluated by colorimetric-MTT and fluorometric-resazurin assays. Varying scrambled-negative control concentrations were applied to HepG2 for assessment of the cytotoxic effect of GalNAc-ASO4 conjugates, and it had no cytotoxic effect on cell viability up to 144 h. GalNAc-ASOs concentrations reducing ABCB1 protein expression after 72 h were detected by western blot. ASOs conjugated with the GalNAc ligand, which specifically targets the liver by binding to asialoglycoprotein receptors in hepatocyte cells, have the potential to increase the effect of anti-cancer therapies by reducing ABCB1 protein expression through gymnotic delivery to cells.

Keywords: ABCB1, antisense oligonucleotides, asialoglycoprotein receptors, gymnosis, hepatocellular carcinoma, *N*-acetylgalactosamine

DOI: 10.1134/S0026893324060050

INTRODUCTION

Hepatocellular carcinoma (HCC) is a primary malignant tumor that develops from hepatocytes due to genetic and environmental factors [1, 2]. Patients with HCC are often diagnosed in advanced stages due to the asymptomatic course and rapid progression of the disease [3]. Although there is currently no effective treatment, there are several treatment options available for HCC [4].

Anti-cancer drugs are often removed from cells through the overexpression of drug transporter systems, a phenomenon known as cancer multidrug resistance (cancer-MDR) [5]. One of the most significant drug transporters associated with cancer-MDR is ATP-binding cassette subfamily B member 1 (ABCB1), also known as multidrug resistance-related protein 1 (MDR1) [6]. This protein also plays a physiological role in preventing harmful compounds from accumulating inside cells [7]. Overexpression of this protein is a significant barrier to treatment, as it

reduces the efficacy of anti-cancer drugs [5, 8]. Therefore, it is one of the most important molecular therapeutic targets to overcome HCC-MDR [9].

Several signaling pathways regulate ABCB1 gene expression [10]. Additionally, the ABCB1 drug transporter has broad substrate specificity and can recognize drugs with varying chemical structures [11]. However, none of the ABCB1 inhibitors used for cancer treatment have shown the desired success in clinical trials, in contrast to preclinical studies [12]. Therefore, an alternative approach is degradation or steric blocking of the target cell's ABCB1 mRNA.

Advances in therapeutic oligonucleotide biotechnology have improved the stability and affinity of modified antisense oligonucleotides (ASOs) [13]. Studies have shown that modifying ASOs with DNA backbone phosphorothioate (PS/PTO) increases their stability [14]. Additionally, it has been reported that adding *N*-acetylgalactosamine (GalNAc) ligands to the 5'- and/or 3'-ends of ASOs provides high-affinity binding to asialoglycoprotein receptors (ASGP-Rs) in hepatocytes, facilitating efficient ASO delivery to the liver. Promising results have been observed in preclinical and ongoing clinical trials using GalNAc-conjugated ASOs for conditions such as NASH and hepatitis B infection [15]. GalNAc-conjugated ASOs offer several advantages, including reduced toxicity and side effects, as well as efficient targeting of hepatocytes [16].

This study performed in silico docking simulations of the designed ASOs against the target ABCB1 mRNA. The in vitro activity for the gymnotic delivery of the ASOs conjugated with the 5'-end GalNAc C3 phosphoramide ligand and modified with DNA backbone PTO in the HepG2 cell line was investigated as hepatocyte targeted ABCB1 inhibitor candidates.

EXPERIMENTAL

Prediction of the secondary and tertiary structures for the target exons of ABCB1 mRNA. The FASTA format sequences of exon 10, exon 17, and exon 20 of the human ABCB1 gene transcript variant 1 mRNA (NM_001348945.2) were acquired from GenBank (NCBI at http://www.ncbi.nlm.nih.gov/nucleotide/). Using the RNAfold server (http://rna.tbi.univie.ac.at/), we predicted the two-dimensional (2D) structure of the exon 10 (192 bp), exon 17 (204 bp), and exon 20 (177 bp) sequences of the ABCB1 gene transcript variant 1 (5586 bp) mRNA. We selected the RNA energy parameter (Turner model, 2004) and obtained results for the minimum free energy (MFE) and thermodynamic statistical ensemble prediction in Vienna format [17]. A dot in dot-bracket notation represents an unmatched position, while a match is represented by parentheses [18]. The centroid secondary structure is defined as the structure with the minimum total base pair distance to all other structures within the thermodynamic ensemble [19].

The three-dimensional (3D) structure of exon 10, exon 17, and exon 20 was predicted using FASTA sequences and 2D structure information. PDB data were retrieved by employing physics- and bioinformatics-based methods through a 3dRNA/DNA server.

Design of ASO sequences for the target ABCB1 mRNA. ASO sequences targeting human ABCB1 gene transcript variant 1 mRNA (NM_001348945.2) were produced using the siRNA Wizard tool (https://www.invivogen.com/sirnawizard/). The GC content was filtered to be within the range of 30–55, resulting in a list of 20-mer target sequences. From the list of siRNA candidates, the first 3 sequences were preferred among the duplexes, with a G at the 5'-end and an A or T at the 3'-end of the sense strand, considering the thermodynamic properties of siRNA. Hairpin and dimer analysis were performed for the selected ASO candidates using the Oligonucleotide Properties Calculator (http://biotools.nubic.northwestern.edu/OligoCalc.html). Additionally, melting temperatures (Tm) were calculated. The candidate ASO sequences were verified to cover all transcript variants of ABCB1 using NCBI Nucleotide BLAST (https://blast.ncbi.nlm.nih.gov/), and an E-value was produced. Furthermore, we performed off-target validation for the human genome. Three ASO sequences (ASO1, ASO2, and ASO3) were selected, including a scrambled-negative control sequence (ASO4) generated from ASO1 using the siRNA Wizard tool.

Secondary structure prediction of ASO sequences. The MaxExpect server (https://rna.urmc.rochester.edu/RNAstructureWeb/Servers/MaxExpect/MaxExpect.html) was used to predict the 2D structures and folding free energies (ΔG) of DNA-ASOs (3'–5'). The 2D structures of single-stranded DNA-ASO sequences (ASO1, ASO2, and ASO3) were achieved by selecting the DNA parameter (Matthews model, 2004) via the RNAfold server (http://rna.tbi.univie.ac.at/) [17].

Hybrid free energy prediction of ASO sequences. The DuplexFold server (https://rna.urmc.rochester.edu/RNAstructureWeb/Servers/DuplexFold/DuplexFold.html) was used to predict the hybrid free energies (HFE) of ASOs (ASO1, ASO2, and ASO3).

Prediction of heat capacity and concentration plot for ASO sequences. The DINAMelt server (http://www.unafold.org/hybrid2.php), a homodimer simulation application, was used to generate concentration (TmConc) and heat capacity (TmCp) graphs for ASOs (ASO1, ASO2, and ASO3).

Tertiary structure prediction of ASO sequences. Using the 2D structure information of DNA-ASOs (3′–5') determined by the RNAfold server (http://rna.tbi.univie.ac.at/) and FASTA sequence, 3D structure prediction of ASOs (ASO1, ASO2, and

ASO3) was performed by the 3dRNA/DNA server (http://biophy.hust.edu.cn/3dRNA) and PDB files were generated.

Predicting the interaction of ASO sequences with target exons of ABCB1 mRNA. The HNADOCK server (http://huanglab.phys.hust.edu.cn/hnadock/) was used to perform nucleic acid docking for RNA-DNA complex structure modeling. The PDB files used were obtained from the prediction of 3D structures of ASO sequences with exon 10 (192 bp), exon 17 (204 bp), and exon 20 (177 bp) sequences of human ABCB1 gene transcript variant 1 mRNA (NM_001348945.2). Using the NGL viewer, the RNA-DNA interactions for the top 10 complex models determined by the DITScoreRR scoring system were visualized.

Kits, chemicals, and solutions. The antisense oligonucleotide sequences were provided by Eurogentec in Germany, while RIPA Buffer (#3924401) and the Protein Marker at 180 kDa (#RM19001) were supplied by Serva Electrophoresis and Abclonal in Germany, respectively. The chemicals used, including 2-mercaptoethanol (#805740) and TEMED (#M110732) from Merck (Germany) and Bovine Serum Albumin (#D1712) from Santa Cruz Biotechnology (Germany), were also included. Capricorn Scientific in Germany provided Dulbecco's PBS (#PBS-10XA), Dulbecco's Modified Eagle's Medium (#DMEM-LPA/HPA), Fetal Bovine Serum (FBS-11B), Penicillin/Streptomycin (#PS-B), and Trypsin-EDTA (#TRY-3B). Wisent Multicell in Canada supplied Sodium Dodecyl Sulfate (#800–100 EG) and Tris (#600–127 EG). Bis-acrylamide (#A2214), Bromphenol Blue (#A2223), Thiazolyl Blue Tetrazolium Bromide (#A3338), and Tween 20 (#A4031) were provided by Biomatik in Canada. The Trypan Blue Solution (#03-102-1B) was provided by Biological Industries, based in Israel. Acrylamide (#A3553) and Resazurin (#R7017) were provided by Sigma-Aldrich, located in the USA. Cell Signaling Technology in the USA provided a Secondary Antibody (#7074P2), MDR1/ABCB1 Primary Antibody (#13342S), Na,K-ATPase alpha1 Primary Antibody (ATP1A1) (#23565S), a Protease/Phosphatase Inhibitor Cocktail (#5872), and an ECL Kit (#6883P3). Ammonium Persulfate (#17874), Bicinchoninic Acid (BCA) Protein Assay Kit (#23225), Polyvinylidene Difluoride Transfer Membrane (#88520), and Skimmed Milk Powder (#LP0033B) were provided by Thermo Fisher Scientific in the USA. Chemicals were acquired from Tekkim in Turkey. The MTT Stock Solution (12 mM) and Resazurin Stock Solution (0.15 mg/mL) were prepared following the protocols from Cold Spring Harbor [20] and bio-protocol [21], respectively. The Western blot solutions were prepared according to Thermo Fisher Scientific's Western Blot Protocols and Recipes.

Synthesis of GalNAc-ASO sequences. The GalNAc C3 phosphoramide carbohydrate ligand was synthesized commercially (Eurogentech, Germany) by adding GalNAc C3 phosphoramide carbohydrate ligand (Glen Research, ABD) in solid phase to the 5'-end of the ASO sequences designed to inhibit target ABCB1 expression. PTO modification was preferred for the bonds between the bases. GalNAc-conjugated PTO-DNA-ASOs were produced by HPLC purification at a 1000 nmol synthesis scale and lyophilized. Stock solutions were prepared from GalNAc-ASOs and stored at −20°C.

HepG2 cell culture condition. The HepG2 (ATCC HB-8065) cells were cultured in DMEM supplemented with 10% FBS, 1% non-essential amino acids, 1% sodium pyruvate, 1% L-glutamine, and 1% penicillin/streptomycin (Sanyo, Japan) with a 1 : 1 ratio of low and high glucose. The flasks were monitored daily, and cells were passaged when the cell density reached 70–80% (Zeiss, Germany). The number of million cells in 1 mL of medium was calculated using trypan blue solution after being able to freeze in 90% FBS + 10% DMSO and stored at −150°C (Sanyo, Japan). The cell density was then determined for cell seeding.

Treatment of HepG2 cells with GalNAc-ASOs. HepG2 cells were seeded in 12-well plates and treated with GalNAc-ASOs (2.5, 5, 10, and 20 μM) 24 h later. Once intermediate stocks were established to give the final concentrations determined, GalNAc-ASOs were delivered directly into the cells by gymnotic delivery (free uptake) without any transfection reagent. Protein isolation was performed 72 h after the GalNAc-ASOs treatment. The protein samples acquired were used in western blot experiments. HepG2 cells were treated with a wider range of GalNAc-ASO4 concentrations (0.625, 1.125, 2.5, 5, 10, and 20 μM), and MTT and resazurin viability assays were performed for up to 144 h.

Determination of ABCB1 protein expression by western blotting. HepG2 cells were treated to a range of GalNAc-ASOs concentrations (2.5, 5, 10, and 20 μM). After 72 h, total protein was extracted from the cells using lysis buffer (RIPA + protease/phosphatase inhibitor) following the kit instructions. The samples were divided and stored at −80°C (New Brunswick Scientific, ABD). Protein concentrations were determined by the BCA assay kit procedure. The concentrations were equalized to 20 μg by plotting the standard curve. To the protein samples, 2X Laemmli buffer was added, and the mixture was denatured at +4°C for 1 h. The denatured protein samples and protein marker (180 kDa) were loaded onto a 4–8% SDS-PAGE mini gel (1mm) and separated at 50V for 5 min, then at 130–150 V for 60 min. The proteins were transferred from the gel to a 0.2 μm PVDF membrane that had been activated with methanol at 100V for 1 h (Mini-PROTEAN Tetra Cell, Bio-Rad). The membrane was then washed with dH_2O four times. After

that, the membrane was blocked with 5% skimmed milk powder in TBS-t at room temperature for 1 h to prevent any non-specific binding. The membranes were cut to cover 130–180 kDa (ABCB1) and 100 kDa (ATP1A1) according to the protein marker. The primary antibody (1 : 1000) was gently shaken with the membranes at room temperature for 3 h to allow for proper binding. Finally, the membranes were rinsed with TBS-t (3 × 10) to remove any excess antibody. The membranes were treated with the secondary antibody (Anti-rabbit IgG, HRP-linked Antibody, 1 : 3000) for one hour at room temperature. Following this, the membranes were washed with TBS-t (3 × 5) and with TBS (2 × 5). The protein bands were visualized using the ECL reagent (ChemiDoc Imaging Systems, Bio-Rad). Protein quantitation was performed using Image Lab Version 6.1 software (Bio-Rad). The results were normalized to the expression of the reference gene (ATP1A1).

MTT cell viability assay. In this experiment, a total of 5000 cells were seeded in 96-well plates with 100 μL medium, in triplicate, for up to 144 h. Control and blank wells were also included. After 24 h, the medium was removed, and GalNAc-ASO4 (0.625, 1.125, 2.5, 5, 10, and 20 μM) was added to the cells to achieve the final concentration. After up to 144 h, MTT stock solution was added at a volume of 10 μL/well, and the plates were incubated at 37°C (Sanyo, Japan). After a 2-h incubation period, the formation of formazan crystals in the wells was observed under a microscope. Once the crystals had formed, the medium was removed, and 100 μL/well of MTT solvent (DMSO) was added. The 96-well plate was shaken for 5 min, and the absorbance was measured at OD570 nm to calculate cell cytotoxicity [Cytotoxicity (%) = (100 × (control – sample)/control)] (EnSpire Multiplate Plate Reader, Perkin Elmer).

Resazurin cell viability assay. In 96-well plates, 5000 cells in 100 μL of medium were seeded in triplicate for up to 144 h, along with control and blank wells. After 24 h, the medium was removed, and GalNAc-ASO4 (0.625, 1.125, 2.5, 5, 10, and 20 μM) was added to the cells. Then, 20 μL/well of resazurin stock solution was added and incubated at 37°C (Sanyo, Japan). After a duration of two h, a fluorescence readout was taken at λ excitation = 530–570 nm (560 nm) and λ emission = 580–620 nm (590 nm). The calculation of cell cytotoxicity was performed [Cytotoxicity (%) = (100 × (control – sample) / control)].

Statistical analysis. The study calculated the mean and standard deviation values of quantitative data and analyzed multiple comparison tests using one-way ANOVA or two-way ANOVA. All statistical analyses were performed using GraphPad Prism 8.0.1 software (GraphPad Software, San Diego, CA, USA). A p value less than 0.05 was considered statistically significant.

RESULTS

The Secondary and Tertiary Structures of the Target Exons of ABCB1 mRNA Were Predicted

The ViennaRNA Web Services (http://rna.tbi.univie.ac.at/) and 3dRNA/DNA Web Server (http://biophy.hust.edu.cn/3dRNA) were used to predict 2D and 3D structures of exon 10 (192 bp, Fig. 1a), exon 17 (204 bp, Fig. 2a), and exon 20 (177 bp, Fig. 3a) of human ABCB1 mRNA transcript variant 1 (5586 bp).

The optimal 2D structure of exon 10, with a MFE of –42.00 kcal/mol in dot bracket notation, is shown in Fig. 1b. The MFE structure drawing of exon 10 encoding base pair probabilities is shown in Fig. 1c. Based on the thermodynamic ensemble prediction, the thermodynamic ensemble free energy is –45.96 kcal/mol. The MFE structure has a frequency of 0.16%. Figure 1d shows the centroid secondary structure of exon 10 in dot bracket notation with a MFE of –23.50 kcal/mol. The optimal 2D structure of exon 17 with a MFE of –48.80 kcal/mol in dot bracket notation is shown in Fig. 2b. The MFE structure drawing of exon 17 encoding base pair probabilities is shown in Fig. 2c. Based on the thermodynamic ensemble prediction, the thermodynamic ensemble free energy is –52.22 kcal/mol. The MFE structure has a frequency of 0.39%. Figure 2d shows the centroid secondary structure of exon 17 in dot bracket notation with an MFE of –33.50 kcal/mol. The optimal 2D structure of exon 20 with a MFE of –29.30 kcal/mol in dot bracket notation is shown in Fig. 3b. The MFE structure drawing of exon 20 encoding base pair probabilities is shown in Fig. 3c. Based on the thermodynamic ensemble prediction, the thermodynamic ensemble free energy is –32.13 kcal/mol. The MFE structure has a frequency of 1.01%. Figure 3d shows the centroid secondary structure of exon 20 in dot bracket notation with a MFE of –14.50 kcal/mol.

The 3dRNA/DNA Web Server can be used to predict 3D structures of long RNA or DNA nucleotide sequences [22]. The study analyzed the sequences of the target exons (exon 10, exon 17, and exon 20) of ABCB1 mRNA to determine the best models since there is no server that predicts 3D structures of a sequence over 3000 nucleotides. Based on the FASTA and 2D structure information of the exons, five 3D structure models were generated using an optimized procedure. The model with the lowest score was selected as the best. The selected models for exons 10, 17, and 20 had scores of 26.6358, 26.4863, and 26.6531, respectively (Figs. 1g, 2g, and 3g).

ASO Candidates for the ABCB1 mRNA Target

ASO sequences targeting human ABCB1 mRNA transcript variant 1 (5586 bp) were identified using InvivoGen's siRNA Wizard™ Online Tool (https://www.invivogen.com/sirnawizard/). The eval-

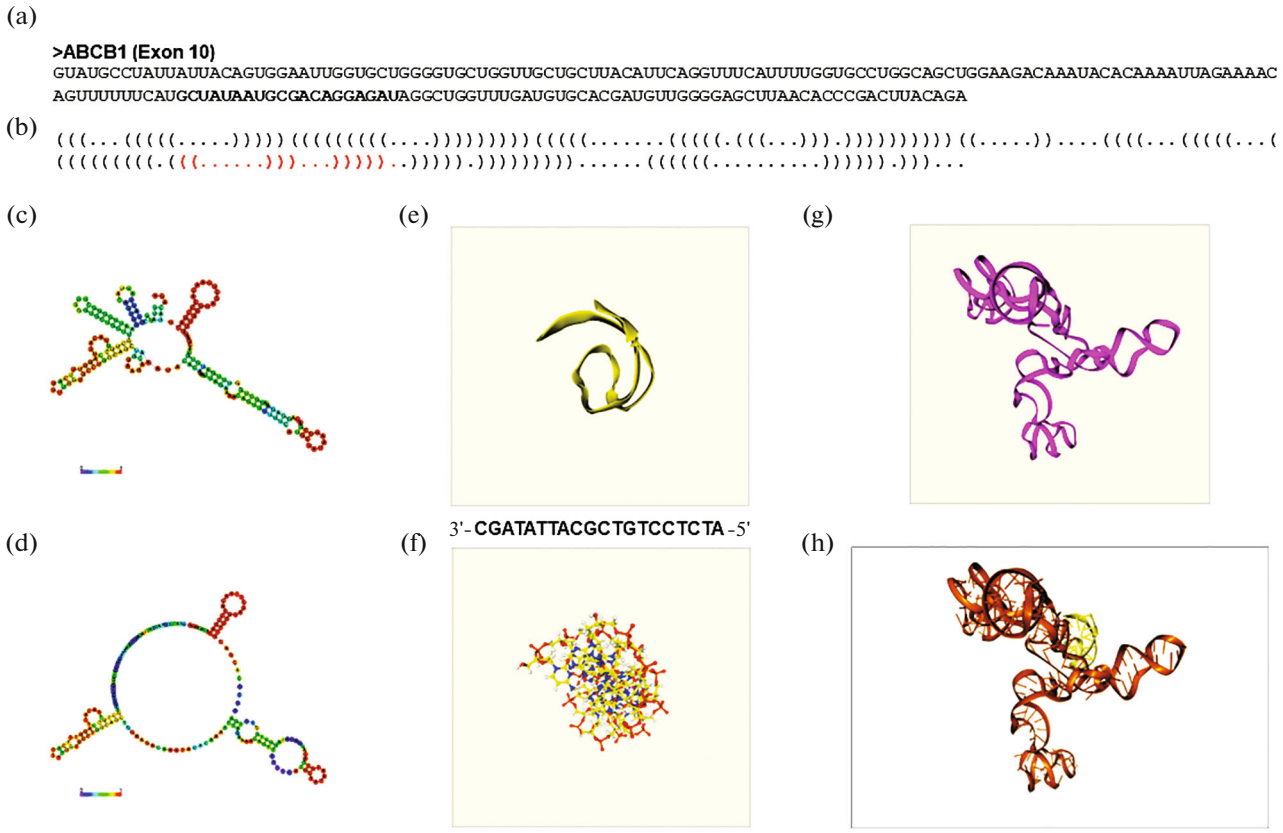

Fig. 1. The prediction of the RNA-DNA interaction of ASO1 with ABCB1 exon 10. (a) FASTA sequence of ABCB1-exon 10 (NCBI, NM_001348945.2). (b) Minimum free energy prediction of ABCB1-exon 10 in dot-bracket (Vienna format, RNAfold web server). (c) MFE secondary structure of ABCB1-exon 10 (−42.00 kcal/mol, RNAfold web server). (d) Centroid secondary structure of ABCB1-exon 10 (−23.50 kcal/mol, RNAfold web server). (e, f) ASO1's tertiary structure prediction (Score: 11.2472, 3dRNA/DNA web server). (g) ABCB1-exon 10's tertiary structure prediction (Score: 26.6358, 3dRNA/DNA web server). (h) The prediction of RNA-DNA interaction of ASO1 with ABCB1-exon 10 (Docking Score: −228.62, Ligand rmsd: 235.61, HNADOCK Server).

uated ASOs included ASO1 targeting exon 10 (192 nt), ASO2 targeting exon 17 (204 nt), ASO3 targeting exon 20 (177 nt), and the scrambled-negative control ASO4 sequences (Table 1).

Based on the Prediction of Secondary Structure, ASO1 Is the Most Suitable Candidate

The MaxExpect Web Server (https://rna.urmc.rochester.edu/RNAstructureWeb/Servers/MaxEx-

Table 1. Sequence information for antisense oligonucleotides

ASO no.	Sense strand (5' → 3')	Anti-sense strand (3' → 5')	Start	*E*-value	GC, %
1	GCTATAATGCGACAGGAGAT	CGATATTACGCTGTCCTCTA	977	0.010	45.00
2	GCCACCACGATAGCTGAAAA	CGGTGGTGCTATCGACTTTT	1958	0.010	50.00
3	GGAGTGTCCGTGGATCACAA	CCTCACAGGCACCTAGTGTT	2526	0.010	55.00
4	GGCATTAGGCAAGTCAATAG	CCGTAATCCGTTCAGTTATC			45.00

The sense strand, anti-sense strand, and GC content were obtained using the siRNA Wizard program. Using NCBI Nucleotide BLAST, start and *E*-value information were acquired

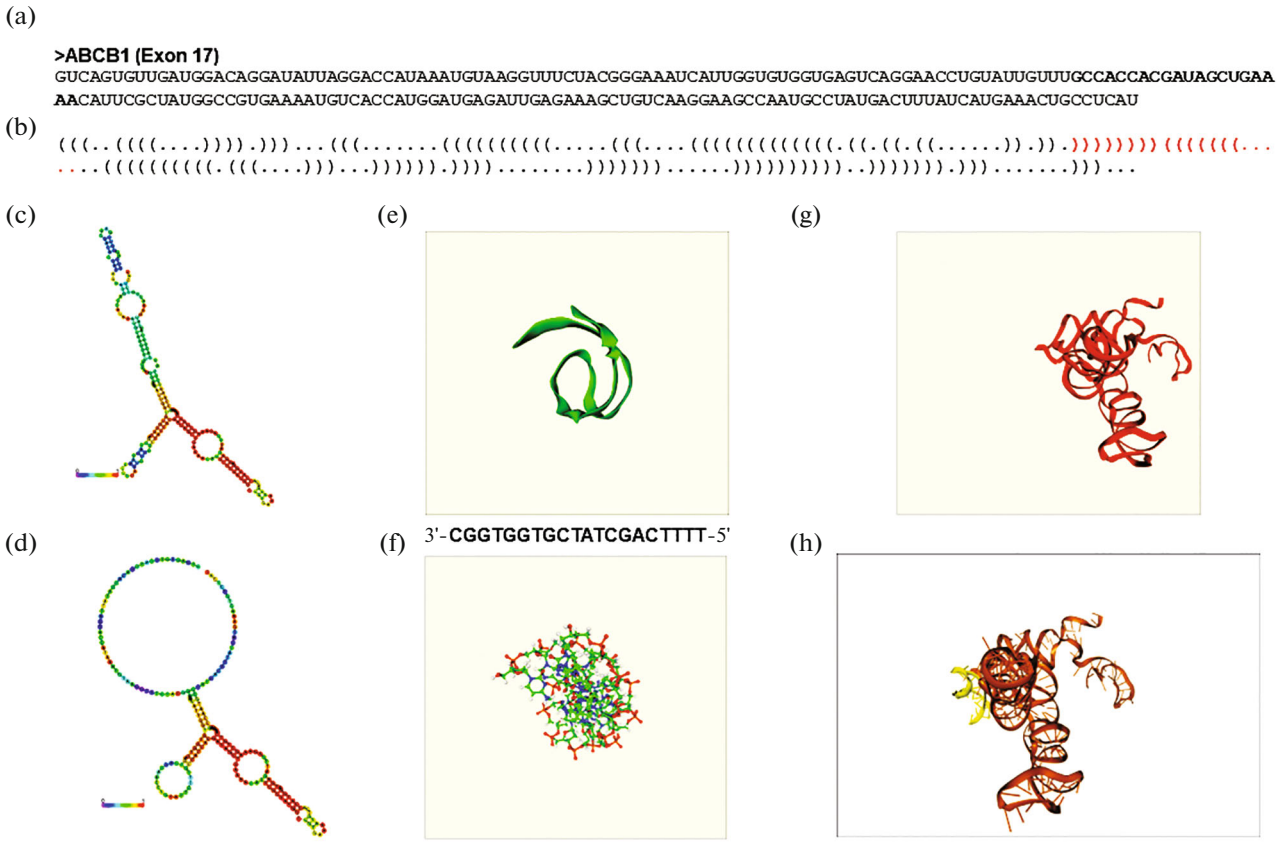

Fig. 2. The Prediction of the RNA-DNA interaction of ASO2 with ABCB1 exon 17. (a) FASTA sequence of ABCB1-exon 17 (NCBI, NM_001348945.2). (b) Minimum free energy prediction of ABCB1-exon 17 in dot-bracket (Vienna format, RNAfold web server). (c) MFE secondary structure of ABCB1-exon 17 (−48.80 kcal/mol, RNAfold web server). (d) Centroid secondary structure of ABCB1-exon 17 (−33.50 kcal/mol, RNAfold web server). (e, f) ASO2's tertiary structure prediction (Score: 6.37399, 3dRNA/DNA web server) (g) ABCB1-exon 17's tertiary structure prediction (Score: 26.4863, 3dRNA/DNA web server). (h) The prediction of RNA-DNA interaction of ABCB1-exon 17 with ASO2 (Docking Score: −121.49, Ligand rmsd: 169.90, HNA-DOCK Server).

pect/MaxExpect.html) was used to predict the 2D structures and free energies of ASOs. ASO1, ASO2, and ASO3 were predicted to have 2D structures with free energy values of 1.6 (Fig. S1a, see Supplementary), 1.4 (Fig. S1e), and 1.3 (Fig. S1i), respectively (see Supplementary). ASO1 was considered the best candidate since the molecule with the highest folding free energy is less likely to fold [23].

Based on the Prediction of Hybrid Free Energy, ASO1 Is the Most Suitable Candidate

The DuplexFold Web Server (https://rna.urmc.rochester.edu/RNAstructureWeb/Servers/DuplexFold/DuplexFold.html) was used to predict the hybrid free energies of ASOs. The predicted folds of ASO1 at −24.5 (Fig. S1b, see Supplementary), ASO2 at −26.2 (Fig. S1f), and ASO3 at −26.6 (Fig. S1j) were based on the HFE conformation. The DuplexFold server facilitates bond formation between molecules with the lowest HFE [24]. Therefore, ASO1 was considered the best candidate because it would have fewer interactions with the molecule that has the highest HFE.

Based on the Prediction of Melting, ASO3 Is the Most Suitable Candidate

The TmConc and the TmCp plots were generated for ASOs using the DINAMelt server (http://www.unafold.org/hybrid2.php). These values were retrieved using the DINAMelt server, which is a widely accepted tool for predicting nucleic acid properties. The results indicate that ASO1 had TmConc and TmCp values of 36.5 and 35.2, respectively (Figs. S1c and S1d, see Supplementary), while ASO2 had TmConc and TmCp values of 50.5 and 41.5, respectively (Figs. S1g and S1h). ASO3 had TmConc values of 65.7 and 54.9 (Figs. S1k and. S1l, see Supplementary). These values are commonly used to predict the melting temperature (Tm) of ASOs, and higher values are generally associated with greater effectiveness in vitro and in vivo [23]. Based on the results obtained with the DINAMelt server, it appears

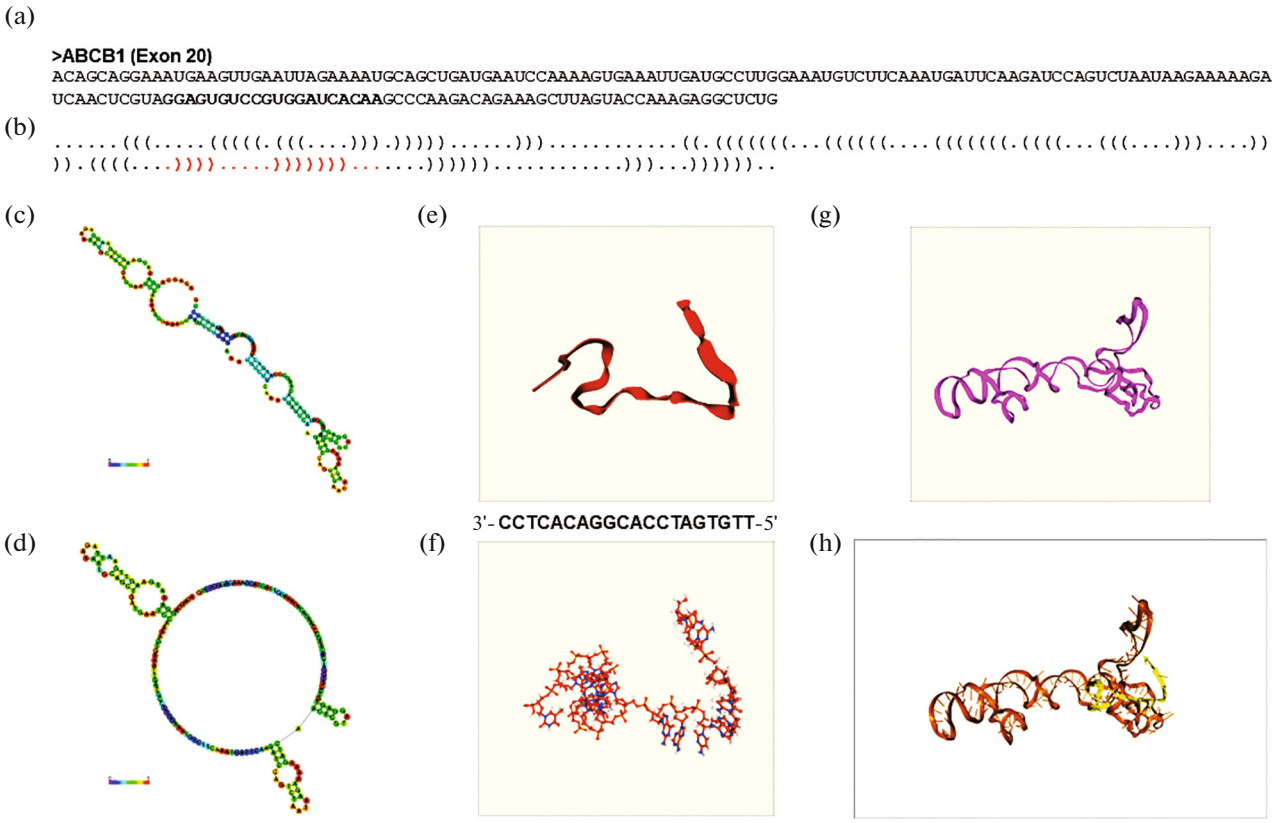

Fig. 3. The prediction of the RNA-DNA interaction of ASO3 with ABCB1 exon 20. (a) FASTA sequence of ABCB1-exon 20 (NCBI, NM_001348945.2). (b) Minimum free energy prediction of ABCB1-exon 20 in dot-bracket (Vienna format, RNAfold web server). (c) MFE secondary structure of ABCB1-exon 20 (−29.30 kcal/mol, RNAfold web server). (d) Centroid secondary structure of ABCB1-exon 20 (−14.50 kcal/mol, RNAfold web server). (e, f) ASO3's tertiary structure prediction (Score: 18.596, 3dRNA/DNA web server) (g) ABCB1-exon 20's tertiary structure prediction (Score: 26.6531, 3dRNA/DNA web server). (h) The prediction of RNA-DNA interaction of ASO3 with ABCB1-exon 20 (Docking Score: −260.03, Ligand rmsd: 355.38, HNA-DOCK Server).

that ASO3 may be the most stable ASO candidate due to its high TmConc and TmCp values.

The Tertiary Structures of the ASO Sequences Were Predicted

The 3D structures of ASO sequences were modeled and scored using the 3dRNA/DNA Web Server (http://biophy.hust.edu.cn/3dRNA). The ASO 3D models with the lowest scores were selected, namely the model with a score of 11.2472 for ASO1 (Figs. 1e and 1f), the model with a score of 6.37399 for ASO2 (Figs. 2e and 2f), and the model with a score of 18.596 for ASO3 (Figs. 3e and 3f).

The Interaction of ASO Sequences with the Target ABCB1 Exons Was Predicted

The RNA-DNA interactions were modeled for exon 10 (192 bp) with ASO1, exon 17 (204 bp) with ASO2, and exon 20 (177 bp) with ASO3 using the HNADOCK Server (http://huanglab.phys.hust.edu.cn/hnadock/). The docking energy score for ASO1 with exon 10 (192 bp) was −228.62, and the ligand rmsd value was 235.61 (Fig. 1h). The results of the RNA-DNA interaction indicate that ASO2 with exon 17 (204 bp) has a docking energy score of −121.49 and a ligand rmsd value of 169.90 (Fig. 2h). Similarly, ASO3 with exon 20 (177 bp) resulted in a docking energy score of −260.03 and a ligand rmsd value of 355.38 (Fig. 3h). Additionally, the HNADOCK server showed higher docking energy scores for exon 20 with ASO3, exon 10 with ASO1, and exon 17 with ASO2, respectively. According to the 2D structure predictions in dot-bracket notation with a MFE, ASO1 has a 10 nt accessibility to the target exon 10 mRNA for hybridization (Figs. 1a and 1b), while ASO2 has a 15 nt accessibility to its target exon 17 mRNA for hybridization (Figs. 2a and 2b). Additionally, ASO3 has an accessibility of 11 nt to its target exon 20 mRNA for hybridization (Figs. 3a and 3b).

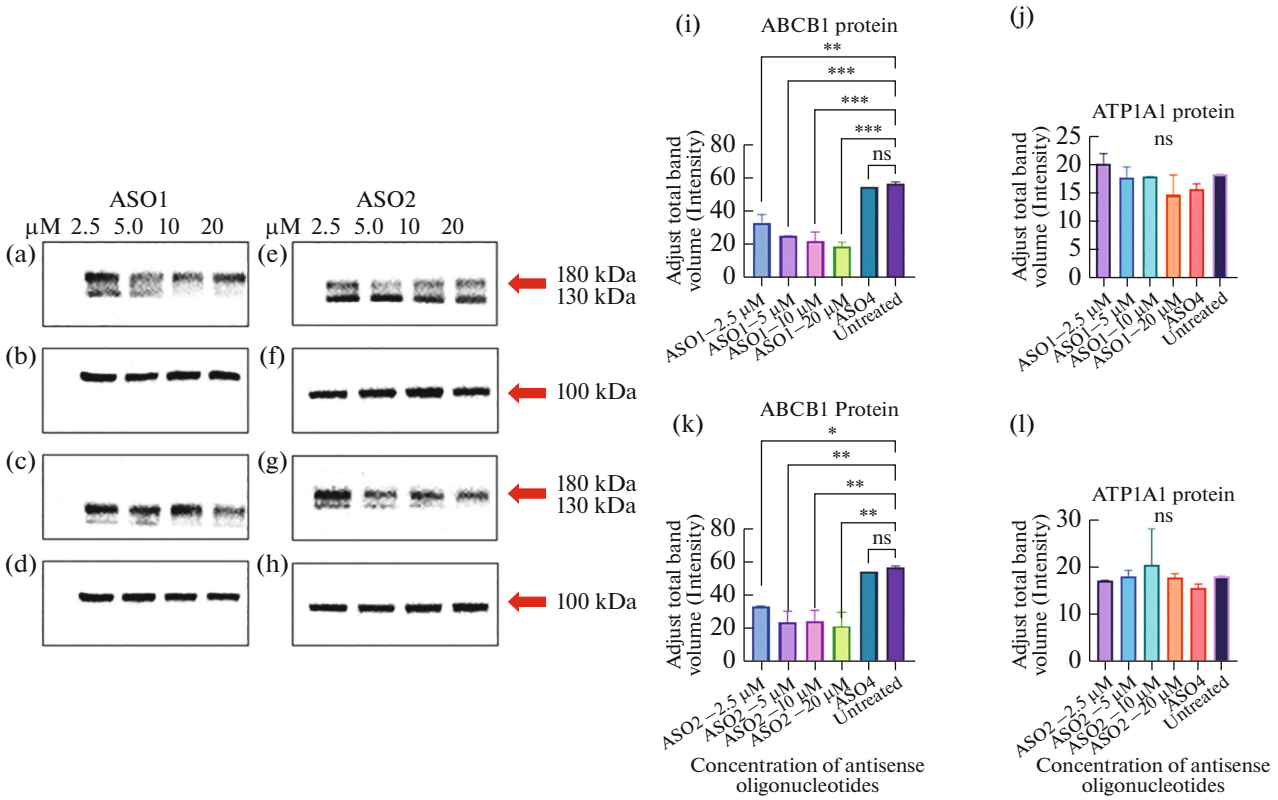

Fig. 4. ABCB1 western blot results of GalNAc-ASO1 and GalNAc-ASO2 treated HepG2 cells (72 h). (a, c) Western blot band images of ABCB1 protein for GalNAc-ASO1 (ChemiDoc MP, Bio-Rad). (b, d) Western blot band images of ATP1A1 protein for GalNAc-ASO1 (ChemiDoc MP, Bio-Rad). (e, g) Western blot band images of ABCB1 protein for GalNAc-ASO2 (ChemiDoc MP, Bio-Rad). (f, h) Western blot band images of ATP1A1 protein for GalNAc-ASO2 (ChemiDoc MP, Bio-Rad). (i) Comparison of ABCB1 western blot band analysis for GalNAc-ASO1 (Untreated vs. ASO1—2.5 μM *P*-Value = 0.0011, Untreated vs. ASO1—5 μM *P*-Value = 0.0002, Untreated vs. ASO1—10 μM *P*-Value = 0.0002, Untreated vs. ASO1 —20 μM *P*-Value = 0.0001). (j) Comparison of ATP1A1 western blot band analysis for GalNAc-ASO1 (ns, not significant). (k) Comparison of ABCB1 western blot band analysis for GalNAc-ASO2 (Untreated vs. ASO2—2.5 μM P Value = 0.0131, Untreated vs. ASO2—5 μM *P*-Value = 0.0025, Untreated vs. ASO2—10 μM *P*-Value = 0.0027, Untreated vs. ASO2—20 μM *P*-Value = 0.0017). (l) Comparison of ATP1A1 western blot band analysis for GalNAc-ASO2 (ns, not significant) (One-way ANOVA, GraphPad Prism 8.0.1. *$p < 0.05$, **$p < 0.01$, ****$p < 0.0001$).

ABCB1 Protein Expression Was Reduced through the Gymnotic Delivery of GalNAc-ASOs

HepG2 cells were treated to different concentrations of GalNAc-ASOs (GalNAc-ASO1, GalNAc-ASO2, and GalNAc-ASO3) and GalNAc-ASO4 (scrambled-negative control), as indicated (2.5, 5, 10, and 20). The western blot band results of the target ABCB1 and reference ATP1A1 proteins after 72 h are presented in Figs. 4a–4h and 5a–5l. In HepG2 cells treated with GalNAc-ASO1, GalNAc-ASO2, and GalNAc-ASO3 (except 2.5 μM), the total band volume of ABCB1 decreased compared to the untreated group (Figs. 4i, 4k, and 5m). Additionally, there was no significant change observed in the total band volume of the reference protein ATP1A1 (Figs. 4j, 4l, and 5n). However, GalNAc-ASO4 did not significantly alter the total band volume of ABCB1 and ATP1A1 (Figs. 5o and 5p). The results indicate that the protein expression of relative ABCB1 decreased with all concentrations of GalNAc-ASO1. Similarly, with GalNAc-ASO2, the protein expression of relative ABCB1 decreased at all concentrations except for 2.5 μM. At a concentration of 10 μM of GalNAc-ASO3, the protein expression of relative ABCB1 also decreased. However, GalNAc-ASO4 did not have any effect on the relative ABCB1 protein expression (Fig. 5r).

GalNAc-ASO4 Did Not Exhibit Cytotoxicity in HepG2 Cells

HepG2 cells were treated to increasing concentrations (0.625, 1.125, 2.5, 5, 10, and 20 μM) of a scrambled-negative control (GalNAc-ASO4). The impact of GalNAc-ASO4 concentrations on cell viability was assessed using Two-way ANOVA (GraphPad Prisim 8.0.1). It was observed that GalNAc-ASO4 did not exhibit any cytotoxic effects in MTT and resazurin viability assays for up to 144 h (Figs. S2a and S2b, see Supplementary).

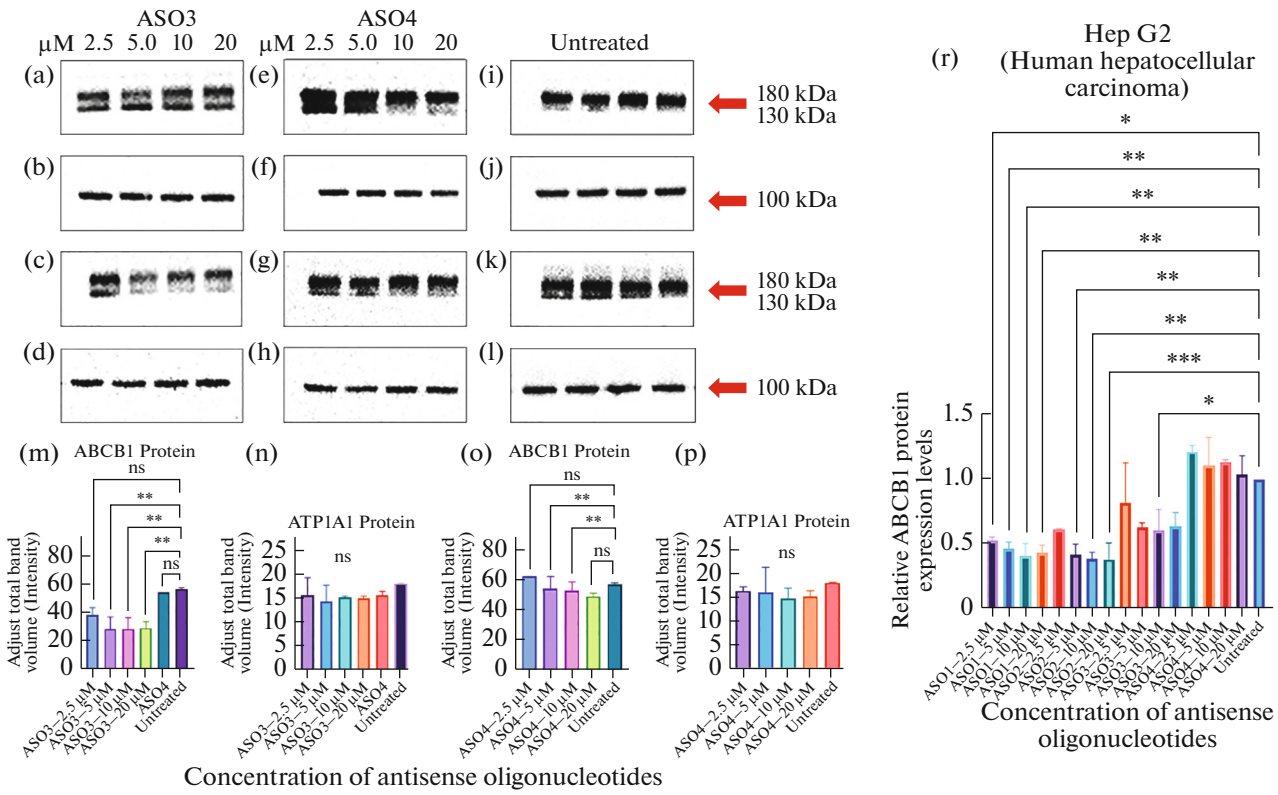

Fig. 5. ABCB1 western blot results of GalNAc-ASO1 treated HepG2 cells (72 h). (a, c) Western blot band images of ABCB1 protein for GalNAc-ASO3 (ChemiDoc MP, Bio-Rad). (b, d) Western blot band images of ATP1A1 protein for GalNAc-ASO3 (ChemiDoc MP, Bio-Rad). (e, g) Western blot band images of ABCB1 protein for GalNAc-ASO4 (ChemiDoc MP, Bio-Rad). (f, h) Western blot band images of ATP1A1 protein for GalNAc-ASO4 (ChemiDoc MP, Bio-Rad). (i, j) Western blot band images of ABCB1 protein for untreated (ChemiDoc MP, Bio-Rad). (k, l) Western blot band images of ABCB1 protein for untreated (ChemiDoc MP, Bio-Rad). (m) Comparison of ABCB1 western blot band analysis for GalNAc-ASO3 (Untreated vs. ASO3—5 μM *P*-Value = 0.0082, Untreated vs. ASO3—10 μM *P*-Value = 0.0084, Untreated vs. ASO3—20 μM *P*-Value = 0.0095). (n) Comparison of ATP1A1 western blot band analysis for GalNAc-ASO3 (ns, not significant). (o) Comparison of ABCB1 western blot band analysis for GalNAc-ASO4 (ns, not significant). (p) Comparison of ATP1A1 western blot band analysis for GalNAc-ASO4 (ns, not significant). (r) Comparison of relative ABCB1 protein expression of GalNAc-ASO concentrations. In Western blot analysis, ABCB1 protein level was normalized to ATP1A1 protein (Untreated vs. ASO1—2.5 M *P*-Value = 0.0118, Untreated vs. ASO1—5 μM *P*-Value = 0.0039, Untreated vs. ASO1—10 μM *P*-Value = 0.0015, Untreated vs. ASO1—20 μM *P*-Value = 0.0023, Untreated vs. ASO2—5 μM *P*-Value = 0.0018, Untreated vs. ASO2—10 μM *P*-Value = 0.0011, Untreated vs. ASO2—20 μM *P*-Value = 0.0010, Untreated vs. ASO3 – 10 μM *P*-Value = 0.0412) (One-way ANOVA, GraphPad Prisim 8.0.1. *$p < 0.05$, **$p < 0.01$, ****$p < 0.0001$).

DISCUSSION

This study investigates the efficacy of GalNAc-conjugated PTO-ASOs designed as ABCB1 inhibitors in HepG2 cells. GalNAc-ASO conjugates selected by in silico analysis were administered to HepG2 cells by gymnotic delivery without using any carrier system, and the effect on ABCB1 protein expression was examined.

In this study, we utilized the PTO-DNA-ASO (20 nt) motif, which was also used in the FDA-approved first-generation antiviral drug, fomivirsen (21 nt) [25]. First-generation ASOs are more resistant to nuclease degradation than PO (phosphodiester)-linked oligonucleotides (ONs). However, their non-specific effects, such as relatively low affinity, limited specificity, and high concentration-dependent toxic effects in vitro, limit their beneficial therapeutic effects in vivo [26, 27].

According to the gymnosis method developed by Stein et al. [28], ASO uptake in cells does not require a carrier system. Modified ASOs enable targeted silencing of adherent or suspended cells in 2D or 3D models, similar to low drug concentrations applied to cells. The authors also reported that ASO-mediated silencing can be sustained for approximately 240 days with little or no toxicity when proper procedures are followed [28].

González-Barriga A. et al. [29] demonstrated through microscopic analysis that ASOs with PTO backbones promote gymnosis. Gymnotic uptake is mediated by clathrin, leading to endosomal-lysosomal accumulation. ASOs delivered to cells via gymnotic delivery have been reported to effectively modulate the

expression of nuclear RNA targets [29]. It is known that gymnotic uptake of ONs with the PTO backbone by cells is a phenomenon that occurs by binding to cell surface proteins driven by disulfide exchange [30]. It has been reported that at least 75% of all phosphate bonds in ASOs require a PTO backbone for cellular uptake to occur [31, 32].

Hillebrand F. et al. [32] showed that modified ASOs can cause the decay of HIV-1 mRNA through gymnotic delivery [32]. Weidner J. et al. [30] demonstrated the effectiveness of antimiRs in gymnotic uptake in 2D and 3D epithelial cell cultures by utilizing sequence length, backbone chemistry, and conjugation strategies [30].

However, Soifer H.S. et al. [33] reported that ONs with unmodified PTO backbones are inactive in in vitro applications unless a carrier vehicle is used [33]. Therefore, in our study, we designed PTO-DNA-ASOs by adding a GalNAc C3 phosphoramide ligand to the 5'-end of the PTO-DNA-ASOs, making them specific to hepatocyte cells. We took advantage of the rapid uptake of ASOs into hepatocyte cells.

Biotechnological efforts to increase the affinity and stability of ASO therapeutics have led to the growing importance of gymnotic delivery and gymnosis in cells [34]. Gymnotic delivery efficiency is guaranteed by modifications at the 3'- and/or 5'-ends, base(s), and backbone level, in addition to the advantages of ASOs due to their small size [35]. Gymnotic delivery is particularly useful when transfection procedures are not feasible. In addition, PTO-ASOs that can be delivered in saline are advantageous in vivo to avoid the additional toxic effects of other formulations, such as lipids [36]. Hillebrand F. et al. [32] reported that LNA-ASOs delivered into cells by gymnosis exhibited the same cytoplasmic distribution as small interfering RNA (siRNAs) delivered via transfection reagents [32]. The transfer of ASOs by gymnosis mediates in vitro simulations that will facilitate the transition to future in vivo experiments.

Prior to conducting the experiments, we utilized computational methods to compare the efficiency of the ASOs we designed [23, 24, 37–39]. We performed molecular docking simulations following the guidelines of in silico protocols developed to increase the success of ASOs [37]. As a result, we determined that ASO1 was the most effective and ASO3 was the most stable under in silico conditions. With regards to exon targeting, ASO3, ASO1, and ASO2 were successful, respectively. ASO1 was selected as the best candidate due to its higher folding free energy compared to other molecules [23]. Considering that ASO1 would interact with the molecule with the higher HFE less frequently, it was thought to be the best candidate. The folding energy prediction and HFE forecasts for ASOs agreed [24]. The Tm of ASOs is often predicted using TmConc and TmCp values. Higher Tm values typically correspond to increased efficacy both in vitro and in vivo [23]. Based on its strong TmConc and TmCp values, ASO3 appears to be the most stable ASO candidate. Additionally, docking energy scores were higher for exon 20 with ASO3, exon 10 with ASO1, and exon 17 with ASO2, in that order. Nevertheless, the incorporation of a PTO backbone modification and GalNAc conjugation to the ASO sequences may result in discrepancies between in vitro and docking outcomes. As indicated by 2D structure predictions in dot-bracket notation with MFE results, exons 17, 20, and 10 were identified as exhibiting greater accessibility for hybridization with ASO2 (15 nt), ASO3 (11 nt), and ASO1 (10 nt), respectively.

The interaction between the ABCB1 mRNA target and ASOs cannot be predicted due to limitations in nucleic acid 3D structure prediction servers, which do not allow analysis of sequences above 3000 nt [22]. Therefore, the efficiency of ASOs was compared using the 3D structures of exons. While these protocols and computational methods have room for improvement, they offer a new opportunity to enhance the selection and success of therapeutic ASOs.

Clinical studies have demonstrated that a 1.5–2 fold increase in ABCB1 expression is indicative of a cancer-MDR phenotype. Markov O.V. et al. [40] demonstrated that a 50% reduction in ABCB1 expression by ONs was enough to restore vinblastine sensitivity in cells [40]. Therefore, in our study, we chose to use GalNAc-modified PTO-ASOs due to the vital physiological role of ABCB1 in the cell. These ASOs have the specificity and willingness to bind specifically to the ASGP-Rs of hepatocytes.

In Soifer H.S. et al. [33] study, adherent HeLa cells were treated with LNA-modified ASO at concentrations of 5 and 10 μM, resulting in the inhibition of Bcl-2 mRNA and protein expression on days 3 and 6 [33]. In our study, we applied a concentration of 10 μM of all GalNAc-ASO conjugates (GalNAc-ASO1, GalNAc-ASO2, GalNAc-ASO3, and GalNAc-ASO4) to HepG2 cells, which led to a decrease in ABCB1 protein expression after 72 h. For all treated concentrations, the GalNAc-ASO4 scrambled-negative control had no adverse effect on both ABCB1 protein expression and cytotoxicity. However, no statistically significant results were found for the 20 μM concentration of GalNAc-ASO3.

Pharmaceutical drugs can act as inhibitors (KEGG DG01622), substrates (KEGG DG01665), or inducers (KEGG DG01893) of ABCB1. Anti-cancer drugs induce hypermethylation of the promoter downstream of ABCB1, leading to a preference for the upstream promoter. Consequently, the expression of ABCB1 increases in cancer cells. Co-treatment with anti-cancer drugs and DNA hypomethylating agents can resensitize the cell to anti-cancer drugs [41]. Therefore, the use of an anti-cancer drug that is not a substrate of ABCB1 or cancer therapies combined with drugs that can inhibit ABCB1 is expected to be successful [42].

Various strategies are being developed to orally deliver ONs instead of intraperitoneally or intravenously, without affecting the gastrointestinal tract [15, 43, 44]. Ionis Pharmaceuticals (2002) administered an ASO molecule orally to humans for the first time as a single dose, in combination with a sodium caprate-based tablet used as a permeation enhancer and tested its plasma bioavailability [45]. Alnylam Pharmaceuticals (2019) reported that administering 3 doses of GalNAc-conjugated siRNA to mice by oral gavage (3 mg/kg) resulted in approximately 90% knockdown of target mRNA for approximately 40 days [43, 46]. Ionis Pharmaceuticals and AstraZeneca (2021) administered a GalNAc-conjugated ON and sodium caprate tablet orally to non-human primates [43]. In the future, it is expected that the bioavailability of GalNAc-ASO therapeutics in oral administration will increase.

In this study, we evaluated the effect of PTO-GalNAc-ASOs on cell viability. However, due to cost constraints, we were unable to include additional modifications that could reduce hepatoxicity. Additionally, we were unable to demonstrate gymnotic delivery to cells by fluorescently labeling the 3'- or 5'-ends. The study has several limitations, including the analysis of protein expression solely through western blot, the use of a single cell line, the restriction to a 2D study, the inability to evaluate the combined effect with tyrosine kinase inhibitors, and the exclusion of other ABC transporter members that may be associated with anticancer drug resistance. However, the preliminary results suggest that GalNAc-ASO conjugates have the potential to inhibit ABCB1 in HCC.

CONCLUSIONS

Hepatocyte-targeted GalNAc-ASO conjugates are considered potential ABCB1 inhibitor candidates for combined treatment options that enhance the effects of anti-cancer drugs and improve survival rates in individuals with advanced HCC. Further studies are needed to demonstrate the therapeutic effect of ABCB1-targeting GalNAc-ASO conjugates with anticancer drugs in 3D cell models and in vivo.

SUPPLEMENTARY INFORMATION

The online version contains supplementary material available at https://doi.org/10.1134/S0026893324060050

ACKNOWLEDGMENTS

We thank the Marmara University Genetic and Metabolic Diseases Research and Application Centre (GEMHAM) for the donation of the HepG2 cell line used in this study.

AUTHOR CONTRIBUTION

Conceptualization: B. Hasturk, F. Eren; Methodology: B. Hasturk, F. Eren; Formal analysis and investigation: B. Hasturk, T. Avsar, S. Ozbas, B. Karademir Yilmaz, F. Eren; Writing: original draft preparation: B. Hasturk, F. Eren; Writing: review and editing: B. Hasturk, T. Avsar, S. Ozbas, B. Karademir Yilmaz, F. Eren; Funding acquisition: B. Hasturk, F. Eren, T. Avsar, B. Karademir Yilmaz; Resources: B. Hasturk, F. Eren; Supervision: F. Eren. All authors commented on previous versions of the manuscript. All authors read and approved the final manuscript.

FUNDING

This work has been supported by Marmara University Scientific Research Projects Coordination Unit under grant number 10587. This study was funded by The Scientific and Technological Research Council of Turkey (TUBITAK) 1002-B Grant no. 222S261.

ETHICS APPROVAL AND CONSENT TO PARTICIPATE

The study utilized with a commercial cell line (Hep G2 [HEPG2], ATCC HB-8065). As this was an in vitro study, ethical approval and informed consent were not required.

CONFLICT OF INTEREST

The authors of this work declare that they have no conflicts of interest.

REFERENCES

1. Llovet J.M., Kelley R.K., Villanueva A., Singal A.G., Pikarsky E., Roayaie S., Lencioni R., Koike K., Zucman-Rossi J., Finn R.S. 2021. Hepatocellular carcinoma. *Nat. Rev. Dis. Primers*. **7** (6), 1–28. https://doi.org/10.1038/s41572-020-00240-3
2. Sukowati C., El-Khobar K.E., Jasirwan C.O.M., Kurniawan J., Gani R.A. 2024. Stemness markers in hepatocellular carcinoma of Eastern vs. Western population: Etiology matters? *Ann. Hepatol*. **29**, 101153. https://doi.org/10.1016/j.aohep.2023.101153
3. Yang J.D., Hainaut P., Gores G.J., Amadou A., Plymoth A., Roberts L.R. 2019. A global view of hepatocellular carcinoma: Trends, risk, prevention and management. *Nat. Rev. Gastroenterol. Hepatol.* **16**, 589–604. https://doi.org/10.1038/s41575-019-0186-y
4. Raza A. 2014. Hepatocellular carcinoma review: Current treatment, and evidence-based medicine. *World J. Gastroenterol*. **20**, 4115. https://doi.org/10.3748/wjg.v20.i15.4115
5. Mansoori B., Mohammadi A., Davudian S., Shirjang S., Baradaran B. 2017. The different mechanisms of cancer drug resistance: A brief review. *Adv. Pharm. Bull*. **7**, 339–348. https://doi.org/10.15171/apb.2017.041
6. Juvale I.I.A., Hamid A.A.A., Halim K.B.A., Has A.T.C. 2022. P-glycoprotein: New insights into

structure, physiological function, regulation and alterations in disease. *Heliyon*. **8**, e09777. https://doi.org/10.1016/j.heliyon.2022.e09777

7. Badiee S.A., Isu U., Khodadadi E., Moradi M. 2023. The alternating access mechanism in mammalian multidrug resistance transporters and their bacterial homologs. *Membranes*. **13**, 568. https://doi.org/10.3390/membranes13060568
8. Emran T.B., Shahriar A., Mahmud A.R., Rahman T., Abir M.H., Siddiquee M.F., Ahmed H., Rahman N., Nainu F., Wahyudin E., Mitra S., Dhama K., Habibullah M.M., Haque S., Islam A., Hassan M.M. 2022. Multidrug resistance in cancer: Understanding molecular mechanisms, immunoprevention and therapeutic approaches. *Front. Oncol*. **12**, 891652. https://doi.org/10.3389/fonc.2022.891652
9. Yin W., Xiang D., Wang T., Zhang Y., Pham C.V., Zhou S., Jiang G., Hou Y., Zhu Y., Han Y., Qiao L., Tran P.H., Duan W. 2021. The inhibition of ABCB1/MDR1 or ABCG2/BCRP enables doxorubicin to eliminate liver cancer stem cells. *Sci. Rep*. **11** (1), 10791. https://doi.org/10.1038/s41598-021-89931-9
10. Sui H., Fan Z.Z., Li Q. 2012. Signal transduction pathways and transcriptional mechanisms of ABCB1/PGP-mediated multiple drug resistance in human cancer cells. *J. Int. Med. Res*. **40**, 426–435. https://doi.org/10.1177/147323001204000204
11. Ceballos M.P., Rigalli J.P., Ceré L.I., Semeñiuk M.B., Catania V.A., Ruiz M.L. 2019. ABC transporters: Regulation and association with multidrug resistance in hepatocellular carcinoma and colorectal carcinoma. *Curr. Med. Chemi*. **26** (7), 1224–1250. https://doi.org/10.2174/0929867325666180105103637
12. Karthika C., Sureshkumar R., Zehravi M., Akter R., Ali F., Ramproshad S., Mondal B., Tagde P., Ahmed Z., Khan F.S., Rahman M.H., Cavalu S. 2022. Multidrug resistance of cancer cells and the vital role of P-Glycoprotein. *Life*. **12**, 897. https://doi.org/10.3390/life12060897
13. Springer A.D., Dowdy S.F. 2018. GalNAC-siRNA conjugates: Leading the way for delivery of RNAI therapeutics. *Nucleic Acid Ther*. **28** (3), 109–118. https://doi.org/10.1089/nat.2018.0736
14. Miller C.M., Harris E.N. 2016. Antisense oligonucleotides: Treatment strategies and cellular internalization. *RNA Dis*. **3** (4), e1393. https://doi.org/10.14800/rd.1393
15. Debacker A.J., Voutila J., Catley M.C., Blakey D.C., Habib N. 2020. Delivery of Oligonucleotides to the Liver with GalNAc. *Mol. Ther*. **28**, 1759–1771. https://doi.org/10.1016/j.ymthe.2020.06.015
16. Cui H., Zhu X., Li S., Wang P., Fang J. 2021. Liver-targeted delivery of oligonucleotides with N-acetylgalactosamine conjugation. *ACS Omega*. **6** (25), 16259–16265. https://doi.org/10.1021/acsomega.1c01755
17. Mathews D.H., Disney M.D., Childs J.L., Schroeder S.J., Zuker M., Turner D.H. 2004. Incorporating chemical modification constraints into a dynamic programming algorithm for prediction of RNA secondary structure. *Proc. Natl. Acad. Sci. U. S. A*. **101**, 7287–7292. https://doi.org/10.1073/pnas.0401799101
18. Lorenz R., Bernhart S.H., Siederdissen C.H.Z., Tafer H., Flamm C., Stadler P.F., Hofacker I.L. 2011. ViennaRNA Package 2.0. *Algorithms Mol. Biol*. **6**, 26. https://doi.org/10.1186/1748-7188-6-26
19. Ding Y., Chan C.Y., Lawrence C.E. 2005. RNA secondary structure prediction by centroids in a Boltzmann weighted ensemble. *RNA*. **11**, 1157–1166. https://rnajournal.cshlp.org/content/11/8/1157
20. 2018. MTT Stock Solution (12 mm). *CSH Protocols*. 2018, pdb.rec096875. https://doi.org/10.1101/pdb.rec096875
21. Sharma N., Arya G., Kumari R., Gupta N., Nimesh S. 2019. Evaluation of anticancer activity of silver nanoparticles on the A549 human lung carcinoma cell lines through alamar blue assay. *Bio Protoc*. **9** (1), e3131. https://doi.org/10.21769/bioprotoc.3131
22. Wang X., Yu S., Lou E., Tan Y.-L., Tan Z.-J. 2023. RNA 3D structure prediction: Progress and perspective. *Molecules*. **28**, 5532. https://doi.org/10.3390/molecules28145532
23. Madanagopal P., Muthukumar H., Thiruvengadam K. 2022. Computational study and design of effective siRNAs to silence structural proteins associated genes of Indian SARS-CoV-2 strains. *Comput. Biol. Chem*. **98**, 107687. https://doi.org/10.1016/j.compbiolchem.2022.107687
24. Al-Madhagi H.A. 2024. Empowering therapeutic strategies against methicillin-resistant staphylococcus aureus riboswitch: Unveiling the potential of small molecules and antisense oligonucleotides through in silico analysis. *Adv. J. Chem. Sect. A*. **7** (1), 15–26. https://doi.org/10.48309/ajca.2024.413428.1405
25. Roush W. 1997. Antisense aims for a renaissance. *Science*. **276**, 1192–1193. https://doi.org/10.1126/science.276.5316.1192
26. Yoo B., Bochkareva E., Bochkarev A., Mou T.C., Gray D.M. 2004. 2'-O-methyl-modified phosphorothioate antisense oligonucleotides have reduced nonspecific effects in vitro. *Nucleic Acids Res*. **32** (6), 2008–2016. https://doi.org/10.1093/nar/gkh516
27. Krieg A.M. 2019. Mind the gap! *Nat. Biotechnol*. **37**, 622–623. https://doi.org/10.1038/s41587-019-0141-z
28. Stein C.A., Hansen J.B., Lai J., Wu S., Voskresenskiy A., Høg A., Worm J., Hedtjärn M., Souleimanian N., Miller P., Soifer H.S., Castanotto D., Benimetskaya L., Ørum H., Koch T. 2010. Efficient gene silencing by delivery of locked nucleic acid antisense oligonucleotides, unassisted by transfection reagents. *Nucleic Acids Res*. **38** (1), e3. https://doi.org/10.1093/nar/gkp841
29. González-Barriga A., Nillessen B., Kranzen J., van Kessel I.D.G., Croes H.J.E., Aguilera B., de Visser P.C., Datson N.A., Mulders S.A.M., van Deutekom J.C.T., Wieringa B., Wansink D.G. 2017. Intracellular distribution and nuclear activity of antisense oligonucleotides after unassisted uptake in myoblasts and differentiated myotubes in vitro. *Nucleic Acid Ther*. **27**, 144–158. https://doi.org/10.1089/nat.2016.0641

30. Weidner J., Kolosionek E., Holmila R., Ax E., Garreau M., Gnerlich F., Olsson H., Czechtizky W., Vollmer S., Rydzik A.M. 2023. Gymnotic uptake of AntimiRs alter microRNA-34a levels in 2D and 3D epithelial cell culture. *Mol. Ther. Nucleic Acids*. **33**, 898–907. https://doi.org/10.1016/j.omtn.2023.08.014

31. Souleimanian N.E., Deleavey G.F., Soifer H.S., Wang S., Tiemann K., Damha M.J., Stein C.A. 2012. Antisense 2'-deoxy, 2'-fluoroarabino nucleic acid (2'F-ANA) oligonucleotides: In vitro gymnotic silencers of gene expression whose potency is enhanced by fatty acids. *Mol. Ther. Nucleic Acids*. **1**, e43. https://doi.org/10.1038/mtna.2012.35

32. Hillebrand F., Ostermann P.N., Müller L., Degrandi D., Erkelenz S., Widera M., Pfeffer K., Schaal H. 2019. Gymnotic delivery of LNA mixmers targeting viral SREs induces HIV-1 mRNA degradation. *Int. J. Mol. Sci.* **20**, 1088. https://doi.org/10.3390/ijms20051088

33. Soifer H.S., Koch T., Lai J.C., Hansen B.R., Hoeg A., Oerum H., Stein C.A. 2011. Silencing of gene expression by gymnotic delivery of antisense oligonucleotides. *Methods Mol. Biol.* **815**, 333–346. https://doi.org/10.1007/978-1-61779-424-7_25

34. Anwar S., Mir F., Yokota T. 2023. Enhancing the effectiveness of oligonucleotide therapeutics using cell-penetrating peptide conjugation, chemical modification, and Carrier-Based delivery strategies. *Pharmaceutics*. **15** (4), 1130. https://doi.org/10.3390/pharmaceutics15041130

35. Blenke E.O., Mahakena S., Fens M.H.A.M., Van Den Dikkenberg J., Hilbrant M., Mastrobattista E. 2020. Impact of chemistry and nanoformulation parameters on cellular uptake and airway distribution of RNA oligonucleotides. *J. Controlled Release*. **317**, 154–165. https://doi.org/10.1016/j.jconrel.2019.11.025

36. Gagnon K.T., Corey D.R. 2019. Guidelines for experiments using antisense oligonucleotides and double-stranded RNAs. *Nucleic Acid Ther.* **29** (3), 116–122. https://doi.org/10.1089/nat.2018.0772

37. Uttarkar A., Babu M., Niranjan V. 2022. Protocol for in-silico design, docking and molecular dynamic simulation of antisense oligonucleotides. Protocols.io. https://doi.org/10.17504/protocols.io.ewov1nr4ogr2/v1

38. Al-Madhagi H.A. 2023. Design of siRNAs against immune-implicated atherosclerosis genes: Computational study. *Turk. Comput. Theor. Chem.* **8** (2), 12–18. https://doi.org/10.33435/tcandtc.1246320

39. Chen E., Ho E.S. 2023. In-silico study of antisense oligonucleotide antibiotics. *PeerJ.* **11**, e16343. https://doi.org/10.7717/peerj.16343

40. Markov O.V., Filatov A.V., Kupryushkin M.S., Chernikov I.V., Patutina O.A., Strunov A.A., Chernolovskaya E.L., Vlassov V.V., Pyshnyi D.V., Zenkova M.A. 2020. Transport oligonucleotides—a novel system for intracellular delivery of antisense therapeutics. *Molecules*. **25** (16), 3663. https://doi.org/10.3390/molecules25163663

41. Skinner K.T., Palkar A.M., Hong A.L. 2023. Genetics of ABCB1 in cancer. *Cancers*. **15**, 4236. https://doi.org/10.3390/cancers15174236

42. Lei Z., Tian Q., Teng Q., Wurpel J.N.D., Zeng L., Pan Y., Chen Z. 2023. Understanding and targeting resistance mechanisms in cancer. *MedComm*. **4** (3), e265. https://doi.org/10.1002/mco2.265

43. Søgaard P.P., Lind M., Christiansen C.R., Petersson K., Clauss A., Caffarel-Salvador E. 2021. Future perspectives of oral delivery of next generation therapies for treatment of skin diseases. *Pharmaceutics.* **13**, 1722. https://doi.org/10.3390/pharmaceutics13101722

44. Afrin H., Bai R.G., Kumar R., Ahmad S.S., Agarwal S.K., Nurunnabi M. 2023. Oral delivery of RNAi for cancer therapy. *Cancer Metastasis Rev*. **42**, 699–724. https://doi.org/10.1007/s10555-023-10099-x

45. Tillman L., Geary R.S., Hardee G.E. 2008. Oral delivery of antisense oligonucleotides in man. *J. Pharm. Sci*. **97**, 225–236. https://doi.org/10.1002/jps.21084

46. BioSpace. 2019. Alnylam announces progress with RNAi therapeutics platform, including oral route of administration and CNS and ocular delivery. https://www.biospace.com/article/releases/alnylam-announces-progress-with-rnai-therapeutics-platform-including-oral-route-of-administration-and-cns-and-ocular-delivery-/.

Publisher's Note. Pleiades Publishing remains neutral with regard to jurisdictional claims in published maps and institutional affiliations.
AI tools may have been used in the translation or editing of this article.